Published in final edited form as:

*Annu Rev Anal Chem (Palo Alto Calif)*. 2018 June 12; 11(1): 287–306. doi:10.1146/annurev-anchem-061417-125935.

# 3D Printed Organ Models for Surgical Applications

**Kaiyan Qiu**, **Ghazaleh Haghiashtiani**, and **Michael C. McAlpine**

Department of Mechanical Engineering, University of Minnesota, Minneapolis, Minnesota 55455, USA

## Abstract

Medical errors are a major concern in clinical practice, suggesting the need for advanced surgical aids for preoperative planning and rehearsal. Conventionally, CT and MRI scans, as well as 3D visualization techniques, have been utilized as the primary tools for surgical planning. While effective, it would be useful if additional aids could be developed and utilized in particularly complex procedures involving unusual anatomical abnormalities that could benefit from tangible objects providing spatial sense, anatomical accuracy, and tactile feedback. Recent advancements in 3D printing technologies have facilitated the creation of patient-specific organ models with the purpose of providing an effective solution for preoperative planning, rehearsal, and spatiotemporal mapping. Here, we review the state-of-the-art in 3D printed, patient-specific organ models with an emphasis on 3D printing material systems, integrated functionalities, and their corresponding surgical applications and implications. Prior limitations, current progress, and future perspectives in this important area are also broadly discussed.

### Keywords

3D printing; organ models; polymeric materials; tissue-mimicking materials; integrated functionalities; surgical applications

## 1. INTRODUCTION

The use of anatomical models and simulators in medicine traces back to centuries ago when clay and stone models were utilized to replicate disease conditions (1, 2). Over the years, the emphasis on decreasing patient mortality, surgical complications, and operation time—accompanied by increased surgical training outside of operating rooms—has driven the evolution of different techniques for surgical planning and training (3, 4). Despite these efforts, one recent study has suggested that “medical errors” lead to a mean death rate of more than 250,000 patients each year, which would result in a rank as the third most prominent cause of death in the United States after heart disease and cancer (5). Indeed, over 4,000 incidents of surgical “never events” (events that should never happen) are estimated to occur annually in the United States alone (6). Hence, effective clinical training and preoperative planning could play a vital role in mitigating these incidents.

**DISCLOSURE STATEMENT**

The authors are not aware of any affiliations, memberships, funding, or financial holdings that might be perceived as affecting the objectivity of this review.

Imaging techniques, such as computed tomography (CT), magnetic resonance imaging (MRI), and 3D virtual visualization, have been employed as critical tools to obtain information regarding patients' anatomies for diagnosis and preoperative planning. However, a precise recognition of orientation and dimension may be obscured in the images, resulting in misinterpretation and on-site improvisation (7). In addition, these tools lack kinesthetic feedback, which is important to quantify and adjust the application of the surgical tools in preoperative rehearsal (8). Developing physical organ models with anatomically accurate features and quantitative feedback could significantly improve the comprehension of surgical target areas in rehearsal and even be used for educating patients. In recent years, rapid prototyping methods, such as 3D printing coupled with 3D imaging techniques, have made the production of such vital models feasible.

In 3D printing processes, parts are manifested layer-by-layer from a 3D representation of the object in a computer-aided design (CAD) program (9). Since the emergence of stereolithography in the 1980s as one of the early 3D printing processes, various techniques have been developed to broaden the application of this technology (9). These 3D printing techniques can be classified into four main categories (10): (*a*) processes based on photopolymerization of liquid polymers or epoxy resins, either by focusing a light source in a predefined pattern on a bath of the liquid-photosensitive material (such as stereolithography, direct light processing, two-photon polymerization, and continuous liquid interface production) or by jetting droplets of the liquid photopolymer followed by curing via an ultraviolet (UV) light source (material jetting or PolyJet); (*b*) processes that involve extruding a thermoplastic filament [fused deposition modeling (FDM)] or viscoelastic materials [direct-write assembly (DWA) or robocasting]; (*c*) processes that create a 3D object from powdered materials via laser sintering, fusion, or use of a binder component, such as selective laser sintering, selective laser melting, electron beam melting, direct metal laser sintering, and binder jetting (powder bed–based inkjet 3D printing); and (*d*) processes that work based on laminating and layering sheet materials, such as laminated object manufacturing and selective deposition lamination.

Today, the application of 3D printing goes well beyond the conventional rapid prototyping of parts for design optimization. In 2016, medical applications comprised approximately 15% of the 3D printing market, making it the third largest market share after consumer products and motor vehicles (11). In this review, we particularly discuss the use of 3D printing for creating patient-specific organ models, with an emphasis on the material systems that can be used in the fabrication process. For this purpose, we review the use of commercial materials, including rigid-plastic, elastomeric (rubber-like), and powder-based materials, as well as customized tissue-mimicking materials for developing organ models and evaluating their efficacy for surgical applications. In addition, we further investigate the incorporation of enhanced functionalities, such as electronics and sensing modules, into the fabrication of these organ models with the purpose of developing advanced surgical aids with quantitative feedback for precision planning.

## 2. 3D PRINTED ORGAN MODELS USING COMMERCiAL MATERIALS

The process of 3D printing patient-specific organ models starts with obtaining the anatomical information of the patient's organ of interest via different imaging modalities, such as CT or MRI scans. These images are normally in a digital imaging and communications in medicine (DICOM) format, which cannot be directly utilized by 3D printers. Therefore, the acquired images need to be postprocessed to first identify the region of interest of the organ via proper segmentation of its volumetric data set (using software such as Vitrea and Mimics) and then generate a stereolithography (STL) file for the 3D printing process (12, 13). In some cases, this STL file needs to be further refined using CAD software packages to rectify the imperfections in the STL model (such as closing the gaps between segments of the model) and optimize its 3D printing (12, 13). The final STL model is then sliced into horizontal layers using 3D slicing software (such as Slic3r) to generate the G-code, which defines the printing pathways to create the 3D printed organ model (Figure 1) (14).

Most of the reported 3D printed organ models are fabricated based on FDM, PolyJet, stereolithography, or inkjet 3D printing technologies and by using commercially available materials (13, 15–19), which can be broadly categorized into rigid-plastic materials, elastomeric (rubber-like) materials, and powder-based materials such as starch/cellulose and plaster.

### 2.1. 3D Printed Organ Models Using Rigid-Plastic Materials

The early 3D printed organ models were mainly fabricated using a limited selection of commercial rigid plastics, primarily involving acrylonitrile butadiene styrene (ABS) and polylactic acid (PLA) thermoplastic filaments for FDM printing, or rigid photopolymers and resins for PolyJet technology (such as the Vero™ family of photopolymers from Stratasys). Such models are still popular due to their accuracy in representing patients' anatomy at a relatively low cost (18). The term rigid-plastic is used here for polymers that have high cross-linking densities and/or high molecular weights with glass transition temperatures ($T_g$) above room temperature. These are mechanically rigid materials with high-impact strength and hardness (20). The Young's moduli for most rigid-plastic materials are close to or within the gigapascal (GPa) range, i.e., at least three orders of magnitude higher than the modulus of soft organ tissue. This discrepancy in the materials' elastic properties relative to the organs themselves limits the direct application and realism of these models for surgical rehearsal (14, 21). Even so, these organ models have demonstrated utility in a variety of medical fields, including cardiology (22–24), urology (25–28), neurology (21, 29, 30), and hepatology (31, 32).

In the field of cardiology, Farooqi et al. (22, 23) 3D printed cardiac models (Figure 2) via an FDM process using ABS filaments. These models accurately replicated the detailed anatomy of a healthy heart (Figure 2*a*) and cases with different congenital heart disease, such as dextro-transposition of the great arteries after performing the Mustard procedure for defect correction (Figure 2*b*). Specifically, it was speculated that the latter model (Figure 2*b*) could have been utilized for optimizing the position of the inflow cannula in the ventricular assist device implantation procedure required for the patient's case (23). In another example,

Schievano et al. (24) created 3D printed models for the right ventricular outflow tract and pulmonary trunk using a thermoplastic polyester resin (P1500 Polyester, Stratasys) via an FDM process. Due to the anatomical accuracy, the models were used to assist two cardiologists participating in the study for more accurate selection of patients for percutaneous pulmonary valve implantation. It was shown that by using the 3D printed models, the accuracy of the selections made by the two cardiologists increased by 8% and 25%, compared to only using MRI scans to make the decisions (24).

In the field of urology, Wake et al. (25) and Kusaka et al. (26) created 3D printed prostate (Figure 2*c*) and kidney models (Figure 2*d*), respectively, via the PolyJet process using the rigid Vero family of photopolymers (Stratasys). These commercial materials are available in a variety of colors, including clear, magenta, and cyan, and can be used to distinguish different printed sections and anatomical details of the organ models (18, 25, 26). The 3D printed models in both works were found to be helpful for recognizing the anatomical features of the organs in the corresponding operations. Komai et al. (27) also fabricated a patient-specific, full-scale 3D printed kidney model via the PolyJet process. The model included a removable tumor combined with its margin, which enabled both the surgeons and patients to envision the kidney before and after tumor resection. It was further confirmed during surgery that the model could be used to help surgeons perform minimally invasive off-clamp partial nephrectomy, because the 3D printed model provided the surgeons with tactile sensation and aided in effectively determining the incision line and angle. In addition, Bernhard et al. (28) created a 3D model of kidney and tumor anatomies via the PolyJet process to educate patients. Specifically, a survey that was conducted in the work indicated that after showing the organ models to the patients, their understanding in the categories of kidney physiology, kidney anatomy, tumor characteristics, and the planned surgical procedure increased by 16.7%, 50%, 39.3%, and 44.6%, respectively.

For neurological applications, Anderson et al. (29) 3D printed hollow intracranial aneurysm models (Figure 2*e*) with rigid walls using an FDM process and PLA filaments. The models could accurately replicate the patients' aneurysm anatomy in a digital subtraction angiography (DSA) image (Figure 2*f*), and therefore they could be used for surgical aid applications as well as for MRI flow phantoms and computational fluid dynamic studies based on rigid models for simulation of aneurysm hemodynamics (29). In another case, Erbano et al. (30) created 3D intracranial aneurysm models using another rigid photosensitive liquid resin, FullCure 720 (Stratasys), via the PolyJet process. The models replicated the accurate location, size, and shape of the intracranial aneurysms, which were identical to the ones measured by DSA. It was concluded that these models can facilitate the selection of surgical procedures and tools (such as aneurysm clips), thus yielding better operational planning for intracranial aneurysms. Wurm et al. (21) initially fabricated rigid cerebral aneurysm models via 3D printing of a photosensitive polymeric liquid-plastic solution using the stereolithography process. The 3D printed models were applied for diagnosis, surgical planning, simulation, training of novice neurosurgeons, and informing patients. All neurosurgeons in the study stated that the 3D printed models were helpful in establishing better comprehension of the cerebrovascular anatomy, as well as the configuration, orientation, and dimension of aneurysms. However, the models were found to

be less beneficial for clipping and dissecting exercises due to the rigid nature of the material used for 3D printing.

In the hepatology field, Zein et al. (31) created 3D printed synthetic liver models from living donors and their respective recipients using the PolyJet process. The 3D printed liver models from donor and recipient accurately mimicked their corresponding native livers (Figures 2*g*,*h*) and were used for anatomical and geometrical evaluations before, during, and after the surgical procedures. The models were found to facilitate the comprehension of the spatial relationship between the vascular and biliary anatomies, as well as enabling hands-on surgical planning and training with the purpose of reducing intraoperative complications. Souzaki et al. (32) also 3D printed a model of a patient's liver with a malignant tumor using the PolyJet process. The model was used for viewing the anatomies and the relative positions of the portal vein, hepatic vein, and tumor, which were identical to the anatomy of the patient's liver. The surgeons utilized the model to evaluate the surgical procedure and determine the resection line for removing the tumor before the operation. The surgical outcome indicated that the tumor was entirely removed and the surgical margin was negative.

### 2.2. 3D Printed Organ Models Using Elastomeric (Rubber-Like) Materials

With the advancement of 3D printing technologies, the palette of materials that can be used in these processes evolved to broaden the applications. This includes the possibility of 3D printing elastomeric (rubber-like) and flexible materials, beyond conventional rigid plastics. Some examples of such materials include the Tango™ family (Stratasys) of photopolymers for PolyJet printing, or thermoplastic elastomer (TPE) filaments such as NinjaFlex® (NinjaTek), SemiFlex™ (NinjaTek), and PolyFlex™ (Polymaker) for FDM printing. In contrast to TPE filaments with elastic properties, rubbers are thermoset polymers with network structures. These thermoset network polymers are not suitable for FDM printing because the polymer chain motion is greatly restricted by a high degree of cross-linking after heating, such that they cannot be remanufactured after their initial heat forming (20). The 3D printable elastomeric (rubber-like) materials have low Young's moduli and good flexibility compared with other 3D printing materials (33). The elasticity and flexibility in these materials are due to the reconfiguration of long chains of the polymers and covalent cross-links. The 3D printed organ models fabricated by such materials provide tactile sensation closer to the actual organ, compared to rigid-plastic materials. Therefore, they allow surgeons to perform different rehearsal operations on them, such as cutting and pressing. Some examples for application of such models in the fields of cardiology (34–37), urology (25, 26), neurology (38, 39, 39a), and pulmonology (40, 41) are discussed below.

For cardiac applications, Yoo et al. (34) created cardiac models with congenital heart disease (Figure 3*a*) using the TangoPlus™ photopolymer via the PolyJet process. The models were used by a total of 81 professionals or trainees for performing the required surgical procedures (Figure 3*a*). Although differences in elasticity and consistency between the model material and human myocardium were noticed by most respondents, 88% of the responses indicated that the quality of the models was acceptable for surgical practice, while 12% found it manageable. In another example, Kiraly et al. (35) fabricated a scaled-up (3×),

flexible, hollow heart model with a congenital defect (Figure 3*b*,*c*). The model was used to guide the surgical approach of arch repair at each step of the operation (Figure 3*b*). The patient operation (Figure 3*c*) was performed following preoperative rehearsal on the 3D printed model (Figure 3*b*), which resulted in increasing the patient's safety, and ultimately, the likelihood of a positive operation outcome. Shiraishi et al. (36) also created a 3D heart model using a stereolithographic biomodeling technique and a photosensitive rubber-like urethane with tensile modulus of 0.01 GPa. The model offered detailed anatomical features and allowed surgeons to cut and suture in preoperative practice due to its rubber-like properties. Furthermore, Yang et al. (37) printed a heart model via the PolyJet process and used the Tango family of photopolymers with different colors to distinguish different parts in the heart model. It was stated that the model not only could be utilized for better visualization of the geometry, but it could also be disassembled for surgical practice, such as a rehearsal for the case of an extended septal myectomy performed in the study.

In the field of urology, Wake et al. (25) 3D printed a patient-specific, cancerous kidney model with accurate anatomy for applications in urological oncology (Figure 3*d*) using a transparent flexible material (HeartPrint™ Flex, Materialise) as the main cortex and the Vero family of rigid photopolymers in different colors as the remaining structures. Such kidney models with tumor sections allowed surgeons to evaluate the complexity of the tumor and its positional relationship with respect to other parts of the organ, thus facilitating the operational planning for partial nephrectomy or ablative therapy. In a real surgical case, the model was used to assist surgeons in the selection of an approach for partial nephrectomy, as well as a resection guidance during the surgery. Kusaka et al. (26) also 3D printed a kidney graft and pelvic cavity model via the PolyJet printing process using mainly the Tango family of photopolymers with different colors. The model was successfully applied for preoperational planning and accurate simulation of the surgical procedure for kidney transplantation.

For neurological applications, Kimura et al. (38) and Khan et al. (39) developed a hollow cerebral aneurysm and a cerebral vasculature physical model by using the Tango family of photopolymers in the PolyJet printing process. In Kimura's work, various types of aneurysm clips were applied on the 3D hollow models (Figure 3*e*) under the operative microscope to optimize the clip placement (38). In Khan's work, the 3D printed cerebral vasculature physical model accurately represented the patient's aneurysm (39). The participating neurosurgical trainees in the study found the models beneficial for better comprehension of the anatomical features of the patients' aneurysm and the corresponding vascular structures, as well as for the determination of proper surgical approach and tools (39). In addition, Wurm et al. (39a) used the PolyJet process to 3D print an aneurysm model. This model was used as a replaceable part for several clipping exercises in microsurgical simulation due to its flexible nature. The model could help neurosurgeons and trainees hone their skills in the clipping approach, clip selection, and clip placement.

In the pulmonology field, Bustamante et al. (40) fabricated 3D printed tracheobronchial tree models (Figure 3*f*) using the PolyJet process. The models were examined with a flexible fiberoptic bronchoscope, and the obtained image (Figure 3*f* ***inset***) from the model was found to be similar to the actual views of the organ during lung isolation. The models were

expected to aid medical professionals to overcome issues in achieving lung isolation via enhanced familiarity with endoscopic bronchial anatomy. In addition, Kurenov et al. (41) 3D printed models of human pulmonary arteries using the TangoPlus photopolymer via the PolyJet process. In terms of anatomy, the models were sufficiently accurate for clinical purposes. In the study, the models were used to design a catheter for regional lung chemotherapy. It was perceived that the applications could be expanded into other areas of clinical care and research for thoracic surgery, such as complex thoracoscopic surgery lobectomies.

### 2.3. 3D Printed Organ Models Using Powder-Based Materials

Powder-based materials such as starch, cellulose, and plaster powder, solidified with binding materials via inkjet 3D printing, have also been evaluated for fabrication of different organ models for surgical applications. Despite the mismatch of their mechanical properties with real organs, such models provide accurate anatomical details with convenient low-cost fabrication. In the field of cardiology, Schmauss et al. (43) demonstrated an example for creating 3D printed cardiac models (Figure 4*a*) using starch/cellulose powder (zp 15e, Z Corporation) and a polymer as the binder (zb 60, Z Corporation) and an elastomeric urethane resin (Por-A-Mold 2030, EnvironMolds, LLC) for further infiltration. The participating surgeons could detect the bypass grafts and their position with respect to the sternum from the model shown in Figure 4*a*. The sterilized model was further used in the operating room for guiding the intraoperative procedures for reopening the sternum (43). In another example, Mottl-Link et al. (7) 3D printed a cardiac model (Figure 4*b*) using plaster-based powder with a binding material. The final model allowed surgeons to obtain intracardiac views that are difficult to achieve during the actual operation. Additionally, the plaster materials were used in neurology applications. Kondo et al. (44) and Oishi et al. (45) developed 3D printed models of a skull base and intracranial tumors using plaster materials. Such models (Figure 4*c*) can provide a better visualization of the anatomy and size of the organ and tumor, and their positional relationships. The models were further used to provide realistic surgical practice and sensation via insertion of surgical instruments under microscopic observation (45).

## 3. LIMITATIONS OF PREVIOUS AND CURRENT 3D PRINTED ORGAN MODELS

Although the aforementioned 3D printed organ models have been useful for surgical planning and rehearsal, the efficacy of these models for applications as advanced surgical aids suffers from two main issues (14). Issue 1: Despite representing the correct anatomy, these 3D printed organ models are incapable of precisely mimicking the physical properties of organ tissue (16), including tactile sensation, mechanical properties (such as elastic modulus, viscoelastic behavior, and hardness), and color. This issue limits their effectiveness in preoperative planning, rehearsal with surgical tools, and other tasks such as pressing, suturing, cutting, clipping, and dissecting (16, 21). This also hampers the ability of 3D printed organ models to accurately predict and replicate organ physical behavior during surgical handling, including deformation and reaction force. Issue 2: These 3D printed organ models lack the functionality to provide quantitative feedback resulting from organ and

tissue handling. This function can be an important add-on for surgical trainers or simulators to aid medical professionals in assessing and controlling their performed tasks quantitatively, such as the amount of pressure applied to the organs via their hands and surgical diagnostic tools.

In the following two sections, we discuss some attempted efforts to address Issue 1 (Section 4) and Issue 2 (Section 5).

## 4. 3D PRINTED ORGAN MODELS USING TISSUE-MIMICKING MATERIALS WITH TAILORED COMPOSITIONS

### 4.1. Previous Work on the Development of Tissue-Mimicking Materials and Organ Models

Tissue-mimicking materials, such as biopolymers (e.g., gelatin, gellan gum, agar, and agarose) and synthetic polymers [e.g., polyurethane, polyvinyl alcohol (PVA), polyvinyl chloride (PVC), room-temperature vulcanizing silicones, and polydimethylsiloxane (PDMS)] (46), have been employed in various arenas of medicine for simulation purposes, including medical imaging modalities (47–49), cardiac strain estimation (50, 51), thermal therapy (52, 53), and surgical simulation and training (54, 55). The composition of these materials can be tailored to replicate the specific properties of soft tissue depending on the application. For instance, phantoms based on polymers such as gelatin (56), agar (57), PVC (46), and PVA (58) have been developed to mimic the acoustic properties (including the speed of sound, acoustic impedance, attenuation, and backscattering coefficient) of soft tissue and were utilized in ultrasound imaging for system calibration, development of new techniques, and training of technicians (47, 59). For developing organ models with implications in surgical planning and training, the composition of the selected material should be modified to closely match the mechanical properties (including elastic modulus, viscoelastic behavior, hardness, ultimate strength, etc.) of the biological soft tissue. Models fabricated with such materials provide more accurate haptic feedback and mechanical behavior, analogous to the real organ.

A common technique for incorporating tissue-mimicking materials in organ models is to first use 3D printing to create a mold and then cast it with tissue-mimicking materials. These molds can be created via one of the following approaches: (*a*) 3D printing a negative mold of the organ and infusing it with the tissue-mimicking material (55, 60–64) or (*b*) employing an approach similar to lost-wax casting, i.e., directly 3D printing the organ model using commercially available materials. This 3D printed model is then used as a template for creating a mold (for example, via silicone molding methods) and the mold cavity is subsequently filled with the tissue-mimicking material to fabricate the final organ model (65–69).

Although molding techniques provide a platform for using customized tissue-mimicking materials and fabricating organ models, they fall short in different aspects that hamper their widespread adaptation for clinical practice. These mold-based fabrication procedures typically involve several steps, which could be time, labor, and cost intensive (29, 34, 70), but they are also prone to the introduction of inaccuracies to the final model (34). In

addition, it is cumbersome, if not impossible, to utilize molding techniques for creating organ models with complex geometries and realistic features, such as incorporating multiple materials to replicate different tissue morphologies within an organ (for instance, cancerous tissue versus healthy tissue in an organ) or encompassing anisotropic properties of tissue. Therefore, the direct 3D printing of tissue-mimicking materials, in lieu of using molding techniques, can appreciably facilitate the fabrication of complex patient-specific organ models with realistic physical properties of tissue. For this purpose, the material should be formulated to have the required tissue-mimicking properties, along with desirable rheological characteristics (such as shear-thinning properties) to facilitate the 3D printing process. While the composition of some of the existing tissue-mimicking materials can be customized for 3D printing (71), they might possess specific properties that do not make them the best candidates for developing organ models for rehearsal with surgical tools. For example, widely used tissue-mimicking materials based on hydrogels, such as gelatin and agar, suffer from limited lifetime, mainly due to the evaporation of their water content over time or bacterial growth (72, 73). In addition, pure gelatin is prone to undesirable damage (73) due to its brittle fracture behavior (74, 75), making it unfavorable for applications in which surgical tools are used. Furthermore, PVA cryogels need to undergo multiple prolonged freeze-thaw cycles (normally over a 12-h cycle) to achieve the required mechanical properties (72, 73, 76). Therefore, developing 3D printable materials with convenient preparation and customization processes to match the properties of the biological tissues is of prime importance.

### 4.2. Development of Customized 3D Printable Polymeric Materials with Patient-Specific Physical Properties for Organ Models

Among the existing 3D printing technologies, DWA conveniently allows the 3D printing of various types of customized materials, including polymer melts, hydrogel and sol-gel precursors, colloidal suspensions, and metallic and semiconducting micro- and nanoparticles (77, 78). In this process, one or more materials of interest, commonly referred to as “inks,” are extruded through fine deposition nozzles under an applied pressure, while a robotic positioning system controls the motion of the nozzle and the printing pathways.

The DWA technique has been previously harnessed to 3D print models of the aortic root from household silicone for conducting surgical training on transapical aortic valve replacement procedures (70, 79). However, these efforts did not involve the customization of the ink material to precisely mimic the properties of tissue. In another recent study, von Rundstedt et al. (80) used two silicone-based inks in a DWA process to 3D print models of patients’ kidneys, including their tumor anatomies. The models were utilized for rehearsal of robot-assisted laparoscopic enucleation of the kidney tumor using the da Vinci® robotic system. It was stated that the inks could mimic the properties of the normal kidney and tumor tissue; however, no characterization results were provided to support this claim.

In a recent work, Qiu et al. (14) developed customized 3D printable polymeric inks with adjustable physical properties to quantitatively match the properties of several patients’ prostate tissues to address Issue 1. First, the anatomical details of the organ were extracted from MRI scans, followed by obtaining the physical properties of the prostate tissue,

including static and dynamic mechanical properties, hardness, and optical reflection (Figure 5*a*). Based on the acquired tissue data, Qiu et al. developed customized polymeric inks that consisted of three main components (Figure 5*b*): (*a*) silicone sealant as an active agent and for stabilizing the structures, (*b*) silicone grease as a bulking agent and for adjusting the softness and flexibility of the material, and (*c*) additives for tuning the color and printability. The developed inks, which replicate the composite nature of human tissue (81, 82), contain several advantages, including adjustable properties, good printability, stable structures, room-temperature vulcanization, convenient preparation, resistance to polymer creep before cross-linking, and good elasticity after cross-linking. The inks also exhibited shear-thinning behavior, which allowed for the extrusion of the inks through fine nozzles (14, 83). The mechanical properties of the inks, which are correlated with changes in the cross-linking density, can be modified by adjusting the primary component ratios to match the mechanical properties of different tissue samples (Figure 5*c*,*d*). Following development of different ink formulations, the fidelity of the physical properties of the printed inks to prostate tissue samples was quantitatively analyzed. The analysis consisted of a series of property comparisons via tests—for static (Figure 5*d*) and dynamic compression, hardness, optical reflection, and density—between the inks and their corresponding tissue samples. The results indicated that the physical properties of the inks could be accurately adjusted to match the properties of the corresponding tissue samples, thus adequately addressing the issue of lacking precise mimicry of real organ tissue.

Furthermore, Qiu et al. (14) utilized their customized inks in a custom-built, DWA 3D printing system to fabricate prostate models based on patients' MRI data. The final 3D printed prostate models showed high anatomical fidelity with their corresponding patient prostate, which was confirmed via surface comparison results obtained from a quantitative 3D registration technique (Figure 5*e*) (14, 84). The high fidelity in physical properties and anatomical structure rendered the 3D printed prostate models capable of predicting the physical behavior of patient organs during surgical handling. To verify the concept, Qiu and coworkers designed both finite element modeling simulations of the patient organ using a third-order Ogden model (85, 86) and compression tests on the 3D printed prostate model via a customized stereo vision system (14, 87, 88) for tracking the deformation. The results confirmed the feasibility of utilizing the 3D printed prostate models for organ physical behavior prediction.

Next, Qiu et al. (14) demonstrated the application of the 3D printed prostate models for surgical rehearsal with diagnostic and surgical tools. For instance, an endoscope was inserted into the urethra of the 3D printed prostate model (Figure 5*f*) to show an unobstructed endoscopic view (Figure 5*g*) on any region of the surface, even under the conditions of pressing or squeezing. Furthermore, with the aid of a surgeon, the researchers performed suturing on the 3D printed prostate models (Figure 5*h*). The models exhibited sufficiently good strength to mitigate excessive damage during these invasive surgical procedures involving needle penetration. Feedback from the participating surgeon indicated that the 3D printed prostate model remained robust during the suturing procedure, without tearing or pulling through of the surgical knot.

Finally, to further establish the merits of the customized polymeric inks, a comparison between the Young's modulus of biological tissues with the developed inks, other tissue-mimicking materials, and commercial rigid-plastic and elastomeric (rubber-like) polymers has been compiled in Figure 6.

## 5. ORGAN MODELS WITH INTEGRATED FUNCTIONALITY

### 5.1. Preliminary Work on Organ Models with Integrated Functionalities

Integration of advanced functionalities, such as electronics and sensing modules, into biological organs or organ simulators has paved new avenues in biomedical research. For instance, the integration of sensing features into organ-on-chip microphysiological models has facilitated the quantitative monitoring of organ responses for drug screening applications (98, 99). In addition, various efforts have been focused on the development of biointegrated electronics that can be mounted on the epidermis or on organs with the purpose of sensing and assessing physiological biomarkers (100–104) or introducing new functionalities, including energy harvesting from the dynamic motions of organs (105, 106).

The same strategy can be adapted for integrating advanced functionalities into physical organ models to broaden their applicability and enhance their efficacy for surgical planning and training. Previous work has shown the feasibility of incorporating such functions into organ models (107, 108). For instance, Laufer et al. (107) integrated force sensors (Figure 7*a*) into a mold-fabricated breast model (Figure 7*a* ***inset***). The developed simulator can be used for measuring the applied force during clinical breast examination and assessing clinical skills and performance (Figure 7*b*). Poniatowski et al. (108) incorporated UV light-sensitive assessment lines into a patient-specific mold-fabricated pyeloplasty simulation model. The lines are not visible under normal light (Figure 7*c*) or endoscopic conditions but can be visualized under UV light (Figure 7*d*). Therefore, with this integrated function, the model can be used to evaluate the twist angle at the anastomosis in training for laparoscopic pyeloplasty using the post-task Black Light Assessment of Surgical Technique (BLAST™).

### 5.2. 3D Printed Prostate Organ Model with Integrated Soft Tactile Sensors for Quantitative Surgical Rehearsal

Qiu et al. (14) successfully incorporated sensing capabilities into their 3D printed prostate models for quantitative surgical rehearsal, which can be expected to address Issue 2. The researchers first fabricated 3D printed soft capacitive tactile sensors (14, 109, 110) that respond to applied pressures in the form of changes in the device capacitances. The sensors consisted of a polyacrylamide-based ionic hydrogel (as electrodes) and a silicone-based dielectric elastomer (the electroactive component) (Figure 8*a*), with the same order of magnitude elastic moduli as the organ model inks (14). The capacitance change and the external applied pressure on the sensor exhibited a linear correlation at a pressure range of 20 to 120 kPa (Figure 8*b*). Therefore, this correlation can be utilized to translate the capacitance change of the sensor to the amount of applied pressure during the application. The 3D printed sensors were then conformally integrated onto the prostate model (Figure 8*c*). Subsequently, a series of quantitative surgical rehearsal applications were conducted on the model. Different surgical tools were applied on the sensors integrated on the outer

surface (Figure 8*d*) and urethra surface (Figure 8*e*) with three quick press-release and three press-hold-release cycles, and the pressure values were deduced from the capacitance changes of the sensor. This capability could be advantageous for medical professionals to quantitatively control the applied pressure and its duration prior to performing the actual procedure.

## 6. PERSPECTIVES

Recently, significant advances in 3D printing organ models and their corresponding surgical applications have been achieved. However, there is still plenty of room for further improvement in the field, and future studies are expected to focus on several different directions (14). First, most 3D printed organ models are static, meaning they lack the ability to simulate dynamic conditions of organ models, such as pulsations of the heart. Therefore, incorporation of convenient and accurate dynamic functionalities (such as actuation) into the organ models will be useful for more realistic surgical rehearsal. Second, although the initial integration of 3D printed soft electronics has been achieved, the functionalities are still limited. For more complicated, multidimensional feedback applications, different types of conformal electronics with more powerful functionalities need to be developed and integrated into the organ models. Third, virtual and assisted reality tools can be used in conjunction with the organ models for visualization of fine features such as vasculature during surgical simulation. Fourth, the 3D printed organ models with integrated functionalities should be evaluated in real-use cases under various operative environments for statistical surveys of surgical outcomes and patient safety to accurately and quantitatively evaluate their effectiveness with large data assessment criteria. Finally, anisotropic properties can possibly be introduced into the 3D printed organ models by controlling the orientation of printing pathways (111, 112) and imbedding fillers (113, 114).

## 7. SUMMARY

The investigation of 3D printed organ models for surgical applications is an important field that may enhance surgical outcomes, reduce medical errors, and improve patient safety. Effort in this area has vastly expanded over the past decade. In this review, we have provided an overview of the most significant progress in the underlying materials research for 3D printing organ models and summarized the corresponding surgical planning and rehearsal applications. This included (*a*) 3D printed organ models using commercial materials, including rigid-plastic materials, elastomeric (rubber-like) materials, and powder-based materials, such as cellulose/starch and plaster, for surgical applications in different medical fields; (*b*) critical limitations of current 3D printed organ models using commercial-grade materials; (*c*) tissue-mimicking materials and their current applications for the development of 3D printed organ models in advanced surgical applications; (*d*) next-generation integrated functionalities on organ models for quantitative feedback; and (*e*) future directions in the field of 3D printed organ models for surgical applications. Indeed, the development of 3D printed patient-specific organ models with physical properties of tissue and integrated functionalities may revolutionize preoperative planning and surgical rehearsal.

## Acknowledgments

The authors acknowledge support from the MnDRIVE RSAM Initiative and the National Institute of Biomedical Imaging and Bioengineering of the National Institutes of Health (NIH) (award 1DP2EB020537). The content is solely the responsibility of the authors and does not necessarily represent the official views of the NIH. G.H. acknowledges support from the graduate school of the University of Minnesota (UMN 2017-18 Interdisciplinary Doctoral Fellowship). The authors thank Dr. Guru Venkatesan and Dr. Nathan Carter for their valuable comments and suggestions during manuscript preparation.

## LITERATURE CITED

1. Owen H. Early use of simulation in medical education. Simul Healthc. 2012; 7:102–16. [PubMed: 22374231]
2. Meller G. A typology of simulators for medical education. J Digit Imaging. 1997; 10:194–96. [PubMed: 9268881]
3. Badash I, Burtt K, Solorzano CA, Carey JN. Innovations in surgery simulation: a review of past, current and future techniques. Ann Transl Med. 2016; 4:453. [PubMed: 28090509]
4. Zevin B, Aggarwal R, Grantcharov TP. Surgical simulation in 2013: Why is it still not the standard in surgical training? J Am Coll Surg. 2014; 218:294–301. [PubMed: 24211055]
5. Makary MA, Daniel M. Medical error—the third leading cause of death in the US. BMJ. 2016; 353:i2139. [PubMed: 27143499]
6. Mehtsun WT, Ibrahim AM, Diener-West M, Pronovost PJ, Makary MA. Surgical never events in the United States. Surgery. 2013; 153:465–72. [PubMed: 23257079]
7. Mottl-Link S, Hübler M, Kühne T, Rietdorf U, Krueger JJ, et al. Physical models aiding in complex congenital heart surgery. Ann Thorac Surg. 2008; 86:273–77. [PubMed: 18573436]
8. Dankowski R, Baszko A, Sutherland M, Firek L, Kalmucki P, et al. 3D heart model printing for preparation of percutaneous structural interventions: description of the technology and case report. Kardiol Pol. 2014; 72:546–51. [PubMed: 24961451]
9. Gross BC, Erkal JL, Lockwood SY, Chen C, Spence DM. Evaluation of 3D printing and its potential impact on biotechnology and the chemical sciences. Anal Chem. 2014; 86:3240–53. [PubMed: 24432804]
10. Low ZX, Chua YT, Ray BM, Mattia D, Metcalfe IS, Patterson DA. Perspective on 3D printing of separation membranes and comparison to related unconventional fabrication techniques. J Membr Sci. 2017; 523:596–613.
11. McWilliams A. Global markets for 3D printing. Wellesley, MA: 2016. Res. Rep. IAS102B, BCC Res.https://www.bccresearch.com/market-research/instrumentation-and-sensors/3d-printing-global-markets-report-ias102b.html
12. Mitsouras D, Liacouras P, Imanzadeh A, Giannopoulos AA, Cai T, et al. Medical 3D printing for the radiologist. Radiographics. 2015; 35:1965–88. [PubMed: 26562233]
13. Giannopoulos AA, Mitsouras D, Yoo SJ, Liu PP, Chatzizisis YS, Rybicki FJ. Applications of 3D printing in cardiovascular diseases. Nat Rev Cardiol. 2016; 13:701–18. [PubMed: 27786234]
14. Qiu K, Zhao Z, Haghiashtiani G, Guo S-Z, He M, et al. 3D printed organ models with physical properties of tissue and integrated sensors. Adv Mater Technol. 2018; 3:1700235. [PubMed: 29608202]
15. Gómez-Ciriza G, Hussain T, Gómez-Cía T, Valverde I. Potential of 3D-printed models in planning structural interventional procedures. Interv Cardiol. 2015; 7:345–52.
16. Rengier F, Mehndiratta A, von Tengg-Kobligk H, Zechmann CM, Unterhinninghofen R, et al. 3D printing based on imaging data: review of medical applications. Int J Comput Assist Radiol Surg. 2010; 5:335–41. [PubMed: 20467825]
17. Marro A, Bandukwala T, Mak W. Three-dimensional printing and medical imaging: a review of the methods and applications. Curr Probl Diagn Radiol. 2016; 45:2–9. [PubMed: 26298798]
18. Vukicevic M, Mosadegh B, Min JK, Little SH. Cardiac 3D printing and its future directions. JACC Cardiovasc Imaging. 2017; 10:171–84. [PubMed: 28183437]

19. Sun Z, Lee SY. A systematic review of 3-D printing in cardiovascular and cerebrovascular diseases. Anatol J Cardiol. 2017; 17:423–35. [PubMed: 28430115]
20. Young RJ, Lovell PA. Introduction to Polymers. Boca Raton, FL: CRC Press; 2011.
21. Wurm G, Tomancok B, Pogady P, Holl K, Trenkler J. Cerebrovascular stereolithographic biomodeling for aneurysm surgery. Technical note. J Neurosurg. 2004; 100:139–45. [PubMed: 14743927]
22. Farooqi KM, Lengua CG, Weinberg AD, Nielsen JC, Sanz J. Blood pool segmentation results in superior virtual cardiac models than myocardial segmentation for 3D printing. Pediatr Cardiol. 2016; 37:1028–36. [PubMed: 27041098]
23. Farooqi KM, Saeed O, Zaidi A, Sanz J, Nielsen JC, et al. 3D printing to guide ventricular assist device placement in adults with congenital heart disease and heart failure. JACC Heart Fail. 2016; 4:301–11. [PubMed: 27033018]
24. Schievano S, Migliavacca F, Coats L, Khambadkone S, Carminati M, et al. Percutaneous pulmonary valve implantation based on rapid prototyping of right ventricular outflow tract and pulmonary trunk from MR data. Radiology. 2007; 242:490–97. [PubMed: 17255420]
25. Wake N, Chandarana H, Huang WC, Taneja SS, Rosenkrantz AB. Application of anatomically accurate, patient-specific 3D printed models from MRI data in urological oncology. Clin Radiol. 2016; 71:610–14. [PubMed: 26983650]
26. Kusaka M, Sugimoto M, Fukami N, Sasaki H, Takenaka M, et al. Initial experience with a tailor-made simulation and navigation program using a 3-D printer model of kidney transplantation surgery. Transplant Proc. 2015; 47:596–99. [PubMed: 25891694]
27. Komai Y, Sugimoto M, Gotohda N, Matsubara N, Kobayashi T, et al. Patient-specific 3-dimensional printed kidney designed for "4D" surgical navigation: a novel aid to facilitate minimally invasive off-clamp partial nephrectomy in complex tumor cases. Urology. 2016; 91:226–33. [PubMed: 26919965]
28. Bernhard JC, Isotani S, Matsugasumi T, Duddalwar V, Hung AJ, et al. Personalized 3D printed model of kidney and tumor anatomy: a useful tool for patient education. World J Urol. 2016; 34:337–45. [PubMed: 26162845]
29. Anderson JR, Thompson WL, Alkattan AK, Diaz O, Klucznik R, et al. Three-dimensional printing of anatomically accurate, patient specific intracranial aneurysm models. J Neurointerv Surg. 2016; 8:517–20. [PubMed: 25862767]
30. Erbano BO, Opolski AC, Olandoski M, Foggiatto JA, Kubrusly LF, et al. Rapid prototyping of three-dimensional biomodels as an adjuvant in the surgical planning for intracranial aneurysms. Acta Cir Bras. 2013; 28:756–61. [PubMed: 24316741]
31. Zein NN, Hanouneh IA, Bishop PD, Samaan M, Eghtesad B, et al. Three-dimensional print of a liver for preoperative planning in living donor liver transplantation. Liver Transpl. 2013; 19:1304–10. [PubMed: 23959637]
32. Souzaki R, Kinoshita Y, Ieiri S, Hayashida M, Koga Y, et al. Three-dimensional liver model based on preoperative CT images as a tool to assist in surgical planning for hepatoblastoma in a child. Pediatr Surg Int. 2015; 31:593–96. [PubMed: 25895074]
33. Loadman MJ. Analysis of Rubber and Rubber-Like Polymers. Amsterdam: Springer; 2012.
34. Yoo SJ, Spray T, Austin EH 3rd, Yun TJ, van Arsdell GS. Hands-on surgical training of congenital heart surgery using 3-dimensional print models. J Thorac Cardiovasc Surg. 2017; 153:1530–40. [PubMed: 28268011]
35. Kiraly L, Tofeig M, Jha NK, Talo H. Three-dimensional printed prototypes refine the anatomy of post-modified Norwood-1 complex aortic arch obstruction and allow presurgical simulation of the repair. Interact Cardiovasc Thorac Surg. 2016; 22:238–40. [PubMed: 26590304]
36. Shiraishi I, Yamagishi M, Hamaoka K, Fukuzawa M, Yagihara T. Simulative operation on congenital heart disease using rubber-like urethane stereolithographic biomodels based on 3D datasets of multislice computed tomography. Eur J Cardiothorac Surg. 2010; 37:302–6. [PubMed: 19758813]
37. Yang DH, Kang JW, Kim N, Song JK, Lee JW, Lim TH. Myocardial 3-dimensional printing for septal myectomy guidance in a patient with obstructive hypertrophic cardiomyopathy. Circulation. 2015; 132:300–1. [PubMed: 26216088]

38. Kimura T, Morita A, Nishimura K, Aiyama H, Itoh H, et al. Simulation of and training for cerebral aneurysm clipping with 3-dimensional models. Neurosurgery. 2009; 65:719–26. [PubMed: 19834377]
39. Khan IS, Kelly PD, Singer RJ. Prototyping of cerebral vasculature physical models. Surg Neurol Int. 2014; 5:11. [PubMed: 24678427]
39a. Wurm G, Lehner M, Tomancok B, Kleiser R, Nussbaumer K. Cerebrovascular biomodeling for aneurysm surgery: simulation-based training by means of rapid prototyping technologies. Surg Innov. 2011; 18:294–306. [PubMed: 21307017]
40. Bustamante S, Bose S, Bishop P, Klatte R, Norris F. Novel application of rapid prototyping for simulation of bronchoscopic anatomy. J Cardiothorac Vasc Anesth. 2014; 28:1122–25. [PubMed: 24332921]
41. Kurenov SN, Ionita C, Sammons D, Demmy TL. Three-dimensional printing to facilitate anatomic study, device development, simulation, and planning in thoracic surgery. J Thorac Cardiovasc Surg. 2015; 149:973–79. [PubMed: 25659851]
42. DELETED IN PROOF
43. Schmauss D, Haeberle S, Hagl C, Sodian R. Three-dimensional printing in cardiac surgery and interventional cardiology: a single-centre experience. Eur J Cardiothorac Surg. 2015; 47:1044–52. [PubMed: 25161184]
44. Kondo K, Harada N, Masuda H, Sugo N, Terazono S, et al. A neurosurgical simulation of skull base tumors using a 3D printed rapid prototyping model containing mesh structures. Acta Neurochir. 2016; 158:1213–19. [PubMed: 27052513]
45. Oishi M, Fukuda M, Yajima N, Yoshida K, Takahashi M, et al. Interactive presurgical simulation applying advanced 3D imaging and modeling techniques for skull base and deep tumors. J Neurosurg. 2013; 119:94–105. [PubMed: 23581591]
46. Li W, Belmont B, Greve JM, Manders AB, Downey BC, et al. Polyvinyl chloride as a multimodal tissue-mimicking material with tuned mechanical and medical imaging properties. Med Phys. 2016; 43:5577–92. [PubMed: 27782725]
47. Culjat MO, Goldenberg D, Tewari P, Singh RS. A review of tissue substitutes for ultrasound imaging. Ultrasound Med Biol. 2010; 36:861–73. [PubMed: 20510184]
48. Lazebnik M, Madsen EL, Frank GR, Hagness SC. Tissue-mimicking phantom materials for narrowband and ultrawideband microwave applications. Phys Med Biol. 2005; 50:4245–58. [PubMed: 16148391]
49. Farrer AI, Odeen H, de Bever J, Coats B, Parker DL, et al. Characterization and evaluation of tissue-mimicking gelatin phantoms for use with MRgFUS. J Ther Ultrasound. 2015; 3:9. [PubMed: 26146557]
50. Langeland S, D'Hooge J, Claessens T, Claus P, Verdonck P, et al. RF-based two-dimensional cardiac strain estimation: a validation study in a tissue-mimicking phantom. IEEE Trans Ultrason Ferroelectr Freq Control. 2004; 51:1537–46. [PubMed: 15600099]
51. Belohlavek M, Bartleson VB, Zobitz ME. Real-time strain rate imaging: validation of peak compression and expansion rates by a tissue-mimicking phantom. Echocardiography. 2001; 18:565–71. [PubMed: 11737965]
52. McDonald M, Lochhead S, Chopra R, Bronskill MJ. Multi-modality tissue-mimicking phantom for thermal therapy. Phys Med Biol. 2004; 49:2767–78. [PubMed: 15285246]
53. Yuan Y, Wyatt C, Maccarini P, Stauffer P, Craciunescu O, et al. A heterogeneous human tissue mimicking phantom for RF heating and MRI thermal monitoring verification. Phys Med Biol. 2012; 57:2021–37. [PubMed: 22430012]
54. Adams F, Qiu T, Mark A, Fritz B, Kramer L, et al. Soft 3D-printed phantom of the human kidney with collecting system. Ann Biomed Eng. 2017; 45:963–72. [PubMed: 27830490]
55. Öpik R, Hunt A, Ristolainen A, Aubin PM, Kruusmaa M. Development of high fidelity liver and kidney phantom organs for use with robotic surgical systems. Presented at IEEE RAS/EMBS Int. Conf. Biomed. Robot. Biomechatron., 4th; Rome. 2012.
56. Cook JR, Bouchard RR, Emelianov SY. Tissue-mimicking phantoms for photoacoustic and ultrasonic imaging. Biomed Opt Express. 2011; 2:3193–206. [PubMed: 22076278]

57. Inglis S, Ramnarine KV, Plevris JN, McDicken WN. An anthropomorphic tissue-mimicking phantom of the oesophagus for endoscopic ultrasound. Ultrasound Med Biol. 2006; 32:249–59. [PubMed: 16464670]
58. Holt RG, Roy RA. Measurements of bubble-enhanced heating from focused, MHz-frequency ultrasound in a tissue-mimicking material. Ultrasound Med Biol. 2001; 27:1399–412. [PubMed: 11731053]
59. Madsen EL, Zagzebski JA, Banjavie RA, Jutila RE. Tissue mimicking materials for ultrasound phantoms. Med Phys. 1978; 5:391–94. [PubMed: 713972]
60. Baba M, Matsumoto K, Yamasaki N, Shindo H, Yano H, et al. Development of a tailored thyroid gland phantom for fine-needle aspiration cytology by three-dimensional printing. J Surg Educ. 2017; 74:1039–46. [PubMed: 28642054]
61. Lurie KL, Smith GT, Khan SA, Liao JC, Ellerbee AK. Three-dimensional, distendable bladder phantom for optical coherence tomography and white light cystoscopy. J Biomed Opt. 2014; 19:36009. [PubMed: 24623158]
62. Shen S, Wang H, Xue Y, Yuan L, Zhou X, et al. Freeform fabrication of tissue-simulating phantom for potential use of surgical planning in conjoined twins separation surgery. Sci Rep. 2017; 7:11048. [PubMed: 28887492]
63. Wang B, Stender B, Long T, Zhang Z, Schlaefer A. An approach to validate ultrasound surface segmentation of the heart. Biomed Eng. 2013; 58(Suppl. 1)doi: 10.1515/bmt-2013-4283
64. Chen SJ, Hellier P, Marchal M, Gauvrit JY, Carpentier R, et al. An anthropomorphic polyvinyl alcohol brain phantom based on Colin27 for use in multimodal imaging. Med Phys. 2012; 39:554–61. [PubMed: 22225325]
65. Kadoya N, Miyasaka Y, Nakajima Y, Kuroda Y, Ito K, et al. Evaluation of deformable image registration between external beam radiotherapy and HDR brachytherapy for cervical cancer with a 3D-printed deformable pelvis phantom. Med Phys. 2017; 44:1445–55. [PubMed: 28214368]
66. Forte AE, Galvan S, Manieri F, Baena FRY, Dini D. A composite hydrogel for brain tissue phantoms. Mater Des. 2016; 112:227–38.
67. Knox K, Kerber CW, Singel SA, Bailey MJ, Imbesi SG. Stereolithographic vascular replicas from CT scans: choosing treatment strategies, teaching, and research from live patient scan data. Am J Neuroradiol. 2005; 26:1428–31. [PubMed: 15956511]
68. Allard L, Soulez G, Chayer B, Qin Z, Roy D, Cloutier G. A multimodality vascular imaging phantom of an abdominal aortic aneurysm with a visible thrombus. Med Phys. 2013; 40:063701. [PubMed: 23718616]
69. Ploch CC, Mansi C, Jayamohan J, Kuhl E. Using 3D printing to create personalized brain models for neurosurgical training and preoperative planning. World Neurosurg. 2016; 90:668–74. [PubMed: 26924117]
70. Kalejs M, von Segesser LK. Rapid prototyping of compliant human aortic roots for assessment of valved stents. Interact Cardiovasc Thorac Surg. 2009; 8:182–86. [PubMed: 19036761]
71. Stein N, Saathoff T, Antoni S-T, Schlaefer A. Creating 3D gelatin phantoms for experimental evaluation in biomedicine. Curr Dir Biomed Eng. 2015; 1:331–34.
72. Pogue BW, Patterson MS. Review of tissue simulating phantoms for optical spectroscopy, imaging and dosimetry. J Biomed Opt. 2006; 11:041102. [PubMed: 16965130]
73. Chmarra MK, Hansen R, Marvik R, Lango T. Multimodal phantom of liver tissue. PLOS ONE. 2013; 8:e64180. [PubMed: 23691165]
74. Czerner M, Fasce LA, Martucci JF, Ruseckaite R, Frontini PM. Deformation and fracture behavior of physical gelatin gel systems. Food Hydrocoll. 2016; 60:299–307.
75. Czerner M, Martucci JF, Fasce LA, Ruseckaite RA, Frontini PM. Mechanical and fracture behavior of gelatin gels. Int Conf Fract. 2013; 6:4439–48.
76. Xie L, Jiang M, Dong XG, Bai X, Tong J, Zhou J. Controlled mechanical and swelling properties of poly(vinyl alcohol)/sodium alginate blend hydrogels prepared by freeze-thaw followed by $Ca^{2+}$ crosslinking. J Appl Polym Sci. 2012; 124:823–31.
77. Lewis JA. Novel inks for direct-write assembly of 3-D periodic structures. Mater Matters. 2008; 3:4–7.
78. Lewis JA. Direct ink writing of 3D functional materials. Adv Funct Mater. 2006; 16:2193–204.

79. Abdel-Sayed P, Kalejs M, von Segesser LK. A new training set-up for trans-apical aortic valve replacement. Interact Cardiovasc Thorac Surg. 2009; 8:599–601. [PubMed: 19282321]
80. von Rundstedt FC, Scovell JM, Agrawal S, Zaneveld J, Link RE. Utility of patient-specific silicone renal models for planning and rehearsal of complex tumour resections prior to robot-assisted laparoscopic partial nephrectomy. BJU Int. 2017; 119:598–604. [PubMed: 27862866]
81. Schuster GA, Schuster TG. The relative amount of epithelium, muscle, connective tissue and lumen in prostatic hyperplasia as a function of the mass of tissue resected. J Urol. 1999; 161:1168–73. [PubMed: 10081863]
82. Huijing PA. Muscle as a collagen fiber reinforced composite: a review of force transmission in muscle and whole limb. J Biomech. 1999; 32:329–45. [PubMed: 10213024]
83. Muth JT, Vogt DM, Truby RL, Menguc Y, Kolesky DB, et al. Embedded 3D printing of strain sensors within highly stretchable elastomers. Adv Mater. 2014; 26:6307–12. [PubMed: 24934143]
84. Shui W, Zhou M, Chen S, Pan Z, Deng Q, et al. The production of digital and printed resources from multiple modalities using visualization and three-dimensional printing techniques. Int J Comput Assist Radiol Surg. 2017; 12:13–23. [PubMed: 27480284]
85. Ogden RW. Large deformation isotropic elasticity: on the correlation of theory and experiment for incompressible rubberlike solids. Proc R Soc A. 1972; 326:565–84.
86. Kim B, Lee SB, Lee J, Cho S, Park H, et al. A comparison among Neo-Hookean model, Mooney-Rivlin model, and Ogden model for chloroprene rubber. Int J Precis Eng Man. 2012; 13:759–64.
87. Bouguet JY. Camera calibration toolbox for Matlab. Calif. Inst. Technol.; Pasadena: 2004. Tech. Rep.
88. Zhang Z. Flexible camera calibration by viewing a plane from unknown orientations. Presented at IEEE Int. Conf. Comp. Vision, 7th; Kerkya, Greece. 1999.
89. Wang B, Borazjani A, Tahai M, Curry AL, Simionescu DT, et al. Fabrication of cardiac patch with decellularized porcine myocardial scaffold and bone marrow mononuclear cells. J Biomed Mater Res A. 2010; 94:1100–10. [PubMed: 20694977]
90. Poornejad N, Frost TS, Scott DR, Elton BB, Reynolds PR, et al. Freezing/thawing without cryoprotectant damages native but not decellularized porcine renal tissue. Organogenesis. 2015; 11:30–45. [PubMed: 25730294]
91. NinjaTek. NinjaFlex® 3D printing filament. NinjaTek; Manheim, PA: 2016. Tech. Spec.https://ninjatek.com/wp-content/uploads/2016/05/NinjaFlex-TDS.pdf
92. NinjaTek. SemiFlex™ 3D printing filament. NinjaTek; Manheim, PA: 2016. Tech. Spec.https://ninjatek.com/wp-content/uploads/2016/05/SemiFlex-TDS.pdf
93. Polymaker. PolyFlex™ 3D printing filament. Polymaker; Shanghai: 2017. Tech. Data Sheethttps://www.lulzbot.com/sites/default/files/PolyFlex_TDS-v1.pdf
94. Baeck K, Lopes P, Verschueren P, Biglino G, Capelli C. State of the art in 3D printing of compliant cardiovascular models: HeartPrint. Material characterization of HeartPrint models and comparison with arterial tissue properties. Presented at Joint Workshop New Technol. Comput. Robot Assist. Surg., 3rd; Verona, Italy. 2013.
95. Objet Geom. Inc.. FullCure®930 TangoPlus. Objet Geom. Inc.; Billerica, MA: 2012. Tech. Data Sheethttp://www.intechrp.com/wp-content/uploads/2012/09/TangoFamily.pdf
96. Stratasys. PolyJet materials. Stratasys; Eden Prairie, MN: 2014. Tech. Data Sheethttp://usglobalimages.stratasys.com/Main/Files/Material_Spec_Sheets/MSS_PJ_PJMaterialsDataSheet.pdf?v=635785205440671440
97. Tymrak BM, Kreiger M, Pearce JM. Mechanical properties of components fabricated with open-source 3-D printers under realistic environmental conditions. Mater Des. 2014; 58:242–46.
98. Lind JU, Busbee TA, Valentine AD, Pasqualini FS, Yuan H, et al. Instrumented cardiac microphysiological devices via multimaterial three-dimensional printing. Nat Mater. 2017; 16:303–8. [PubMed: 27775708]
99. Zhang YS, Aleman J, Shin SR, Kilic T, Kim D, et al. Multisensor-integrated organs-on-chips platform for automated and continual in situ monitoring of organoid behaviors. PNAS. 2017; 114:E2293–302. [PubMed: 28265064]
100. Yeo W-H, Webb RC, Lee W, Jung S, Rogers JA. Bio-integrated electronics and sensor systems. Proc SPIE 8725. 2013. Micro- Nanotechnol. Sensors Syst. Appl. V, 872511.

101. Zhang YH, Webb RC, Luo HY, Xue YG, Kurniawan J, et al. Theoretical and experimental studies of epidermal heat flux sensors for measurements of core body temperature. Adv Healthc Mater. 2016; 5:119–27. [PubMed: 25953120]
102. Guo SZ, Qiu K, Meng F, Park SH, McAlpine MC. 3D printed stretchable tactile sensors. Adv Mater. 2017; 29:1701218.
103. Mannoor MS, Tao H, Clayton JD, Sengupta A, Kaplan DL, et al. Graphene-based wireless bacteria detection on tooth enamel. Nat Commun. 2012; 3:763. [PubMed: 22453836]
104. Xu L, Gutbrod SR, Bonifas AP, Su Y, Sulkin MS, et al. 3D multifunctional integumentary membranes for spatiotemporal cardiac measurements and stimulation across the entire epicardium. Nat Commun. 2014; 5:3329. [PubMed: 24569383]
105. Dagdeviren C, Yang BD, Su Y, Tran PL, Joe P, et al. Conformal piezoelectric energy harvesting and storage from motions of the heart, lung, and diaphragm. PNAS. 2014; 111:1927–32. [PubMed: 24449853]
106. Lu B, Chen Y, Ou D, Chen H, Diao L, et al. Ultra-flexible piezoelectric devices integrated with heart to harvest the biomechanical energy. Sci Rep. 2015; 5:16065. [PubMed: 26538375]
107. Laufer S, Rasske K, Stopfer L, Kurzynski C, Abbott T, et al. Fabric force sensors for the clinical breast examination simulator. Stud Health Technol Inform. 2016; 220:193–98. [PubMed: 27046577]
108. Poniatowski LH, Wolf JS Jr, Nakada SY, Reihsen TE, Sainfort F, Sweet RM. Validity and acceptability of a high-fidelity physical simulation model for training of laparoscopic pyeloplasty. J Endourol. 2014; 28:393–98. [PubMed: 24320223]
109. Robinson SS, O'Brien KW, Zhaob H, Peele BN, Larson CM, et al. Integrated soft sensors and elastomeric actuators for tactile machines with kinesthetic sense. Extreme Mech Lett. 2015; 5:47–53.
110. Sun JY, Keplinger C, Whitesides GM, Suo Z. Ionic skin. Adv Mater. 2014; 26:7608–14. [PubMed: 25355528]
111. Johnson BN, Lancaster KZ, Zhen G, He J, Gupta MK, et al. 3D printed anatomical nerve regeneration pathways. Adv Funct Mater. 2015; 25:6205–17. [PubMed: 26924958]
112. Zou R, Xia Y, Liu SY, Hu P, Hou WB, et al. Isotropic and anisotropic elasticity and yielding of 3D printed material. Compos Pt B Eng. 2016; 99:506–13.
113. Gnanasekaran K, Heijmans T, van Bennekom S, Woldhuis H, Wijnia S, et al. 3D printing of CNT- and graphene-based conductive polymer nanocomposites by fused deposition modeling. Appl Mater Today. 2017; 9:21–28.
114. Valentine AD, Busbee TA, Boley JW, Raney JR, Chortos A, et al. Hybrid 3D printing of soft electronics. Adv Mater. 2017; 29:1703817.

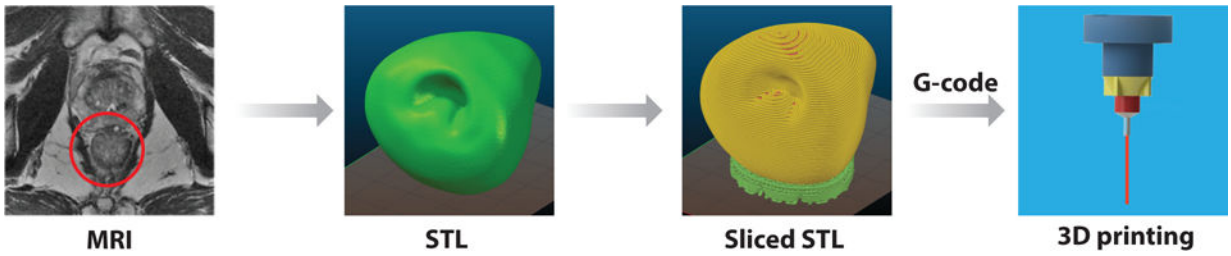


**Figure 1.**

The general procedure for converting a magnetic resonance imaging (MRI) scan of a patient's organ (a prostate in this figure) to G-code for the process of 3D printing a patient-specific organ model from a stereolithography (STL) file. Adapted with permission from Reference 14. Copyright 2017, John Wiley & Sons.

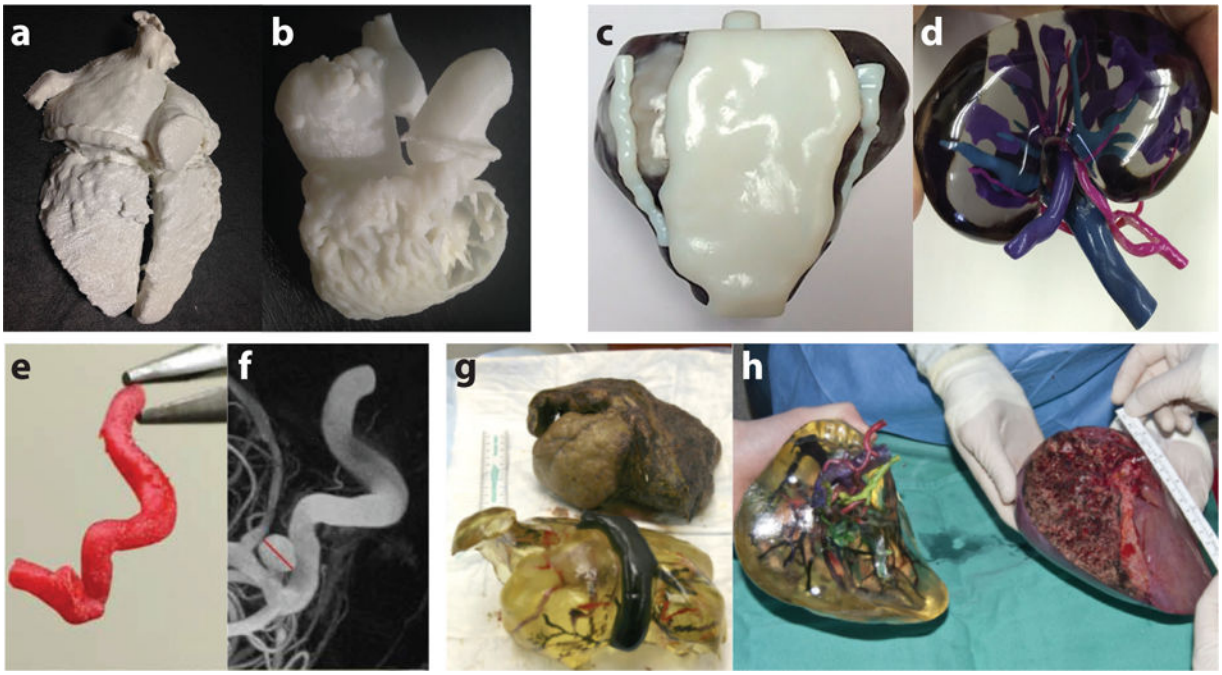


**Figure 2.**

3D printed organ models using rigid-plastic materials. (*a*) A 3D printed cardiac model without congenital disease and (*b*) a 3D printed cardiac model after the Mustard procedure for correcting the congenital heart defect using a commercial ABS thermoplastic filament for printing. Panel *a* adapted with permission from Reference 22. Copyright 2016, Springer Nature. Panel *b* adapted with permission from Reference 23. Copyright 2016, American College of Cardiology Foundation. (*c*) A 3D printed prostate model and (*d*) a 3D printed kidney model using the Vero™ family of polymers. Panel *c* adapted with permission from Reference 25. Copyright 2016, Royal College of Radiologists. Panel *d* adapted with permission from Reference 26. Copyright 2015, Elsevier. (*e*) A 3D printed intracranial aneurysm model using polylactic acid as the rigid walls and (*f*) its corresponding digital subtraction angiography image for patient aneurysm. Panels adapted with permission from Reference 29. Copyright 2016, British Medical Journal. (*g*) A 3D printed liver model and (*h*) a right liver lobe model using the PolyJet process and their corresponding actual organs. Panels adapted with permission from Reference 31. Copyright 2013, American Association for the Study of Liver Diseases.

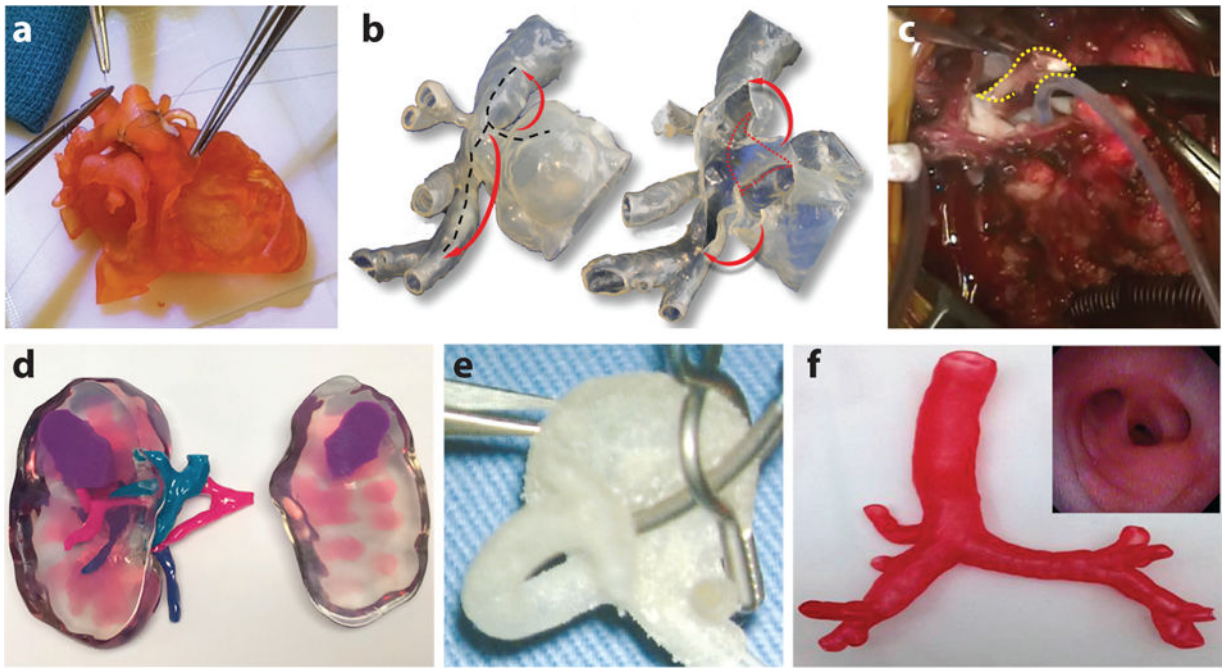


**Figure 3.**

3D printed organ models using elastomeric (rubber-like) materials. (*a*) A 3D printed cardiac model with a congenital defect using the TangoPlus™ photopolymer for hands-on surgical training. Adapted with permission from Reference 34. Copyright 2017, American Association for Thoracic Surgery. (*b*) A 3D printed hollow aortic arch model. The black dotted lines, red dotted lines, and red arrows represent the proposed incision lines, the internal obstructive ridge to be resected after opening the model, and arch augmentation, respectively. Adapted with permission from Reference 35. Copyright 2016, Oxford University Press. (*c*) The obstructive ridge is resected (*yellow dotted line*) in a real operation, guided via simulation on the corresponding 3D printed model in *b*. Adapted with permission from Reference 35. Copyright 2016, Oxford University Press. (*d*) A 3D printed kidney model using flexible material as the kidney's main cortex showing the relative position of the renal tumor with respect to the renal artery, vein, and collecting system. Adapted with permission from Reference 25. Copyright 2016, Royal College of Radiologists. (*e*) A 3D printed left middle cerebral bifurcation aneurysm for surgical clipping rehearsal. Adapted with permission from Reference 38. Copyright 2009, Oxford University Press. (*f*) A 3D printed tracheobronchial tree model. (*Inset*) Fiberoptic view of the 3D printed tracheobronchial tree model through the bronchus intermedius. Adapted with permission from Reference 40. Copyright 2014, Elsevier.

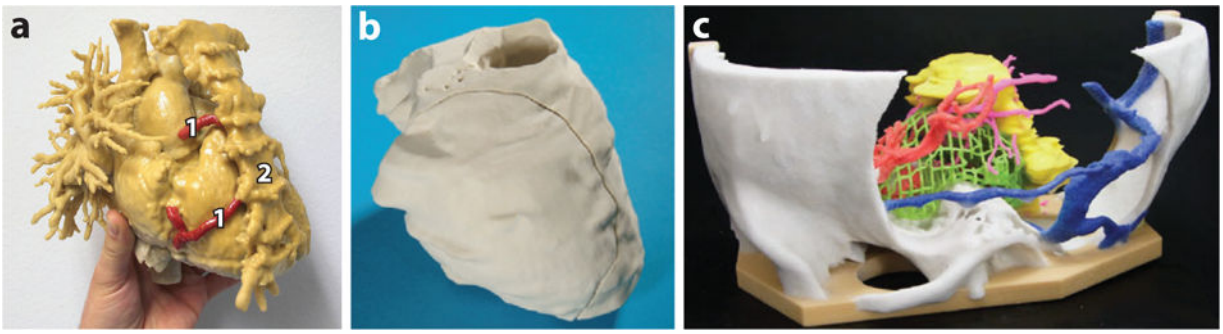


**Figure 4.**

3D printed organ models using powder-based materials. (*a*) A 3D printed cardiac model using starch/cellulose showing the relative position of the right coronary artery bypass graft (shown in red and labeled 1) with respect to the patient's sternum (labeled 2). Adapted with permission from Reference 43. Copyright 2014, Oxford University Press. (*b*) A 3D printed cardiac model using plaster. Adapted with permission from Reference 7. Copyright 2008, Elsevier. (*c*) A 3D printed skull model with a mesh tumor using plaster. Adapted with permission from Reference 44. Copyright 2016, Springer Nature.

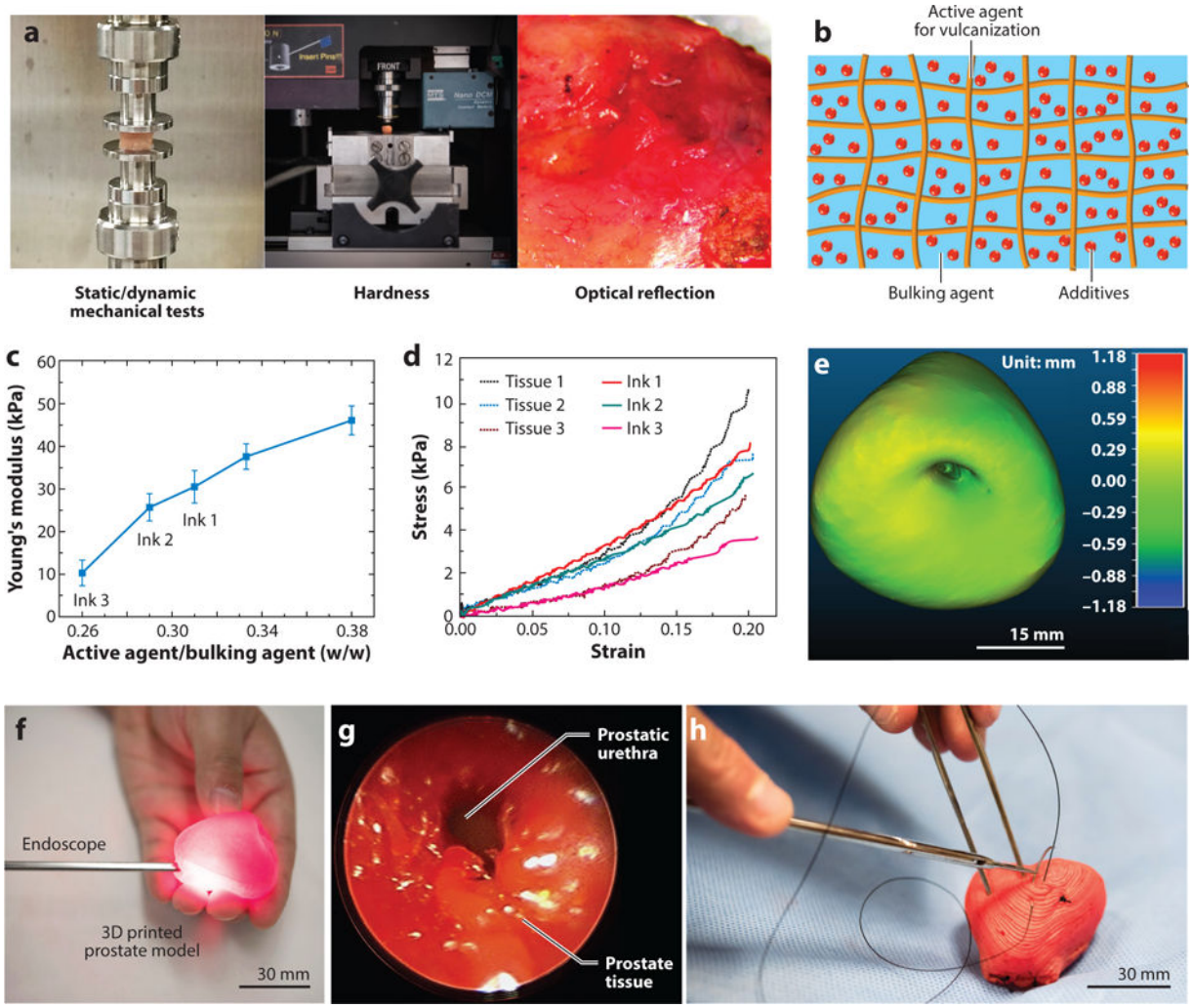


**Figure 5.**

Development of customized polymeric inks with physical properties mimicking patient tissue samples for 3D printing of prostate models and their corresponding surgical rehearsal. (*a*) Mechanical and optical tests for obtaining the physical and optical properties of human patient prostate tissue samples to guide the ink development process. (*b*) Schematic of the composite structure of the customized polymeric inks. (*c*) A plot of primary component weight ratios versus Young's moduli for the customized polymeric inks. (*d*) Static compression fidelity via stress-strain curves between different patient prostate tissue samples (Tissue 1, 2, 3) and samples of customized polymeric inks (Ink 1, 2, 3). (*e*) Calibrated distance map via 3D registration for comparison of anatomical fidelity (difference in mm) between a patient prostate and a 3D printed prostate model. (*f*) Surgical rehearsal demonstration with an endoscope inserted into the urethra of the 3D printed prostate model. (*g*) Endoscopic view of the urethra inside of the prostate model. (*h*) Surgical suturing demonstration on the 3D printed prostate model. Figure adapted with permission from Reference 14. Copyright 2017, John Wiley & Sons.

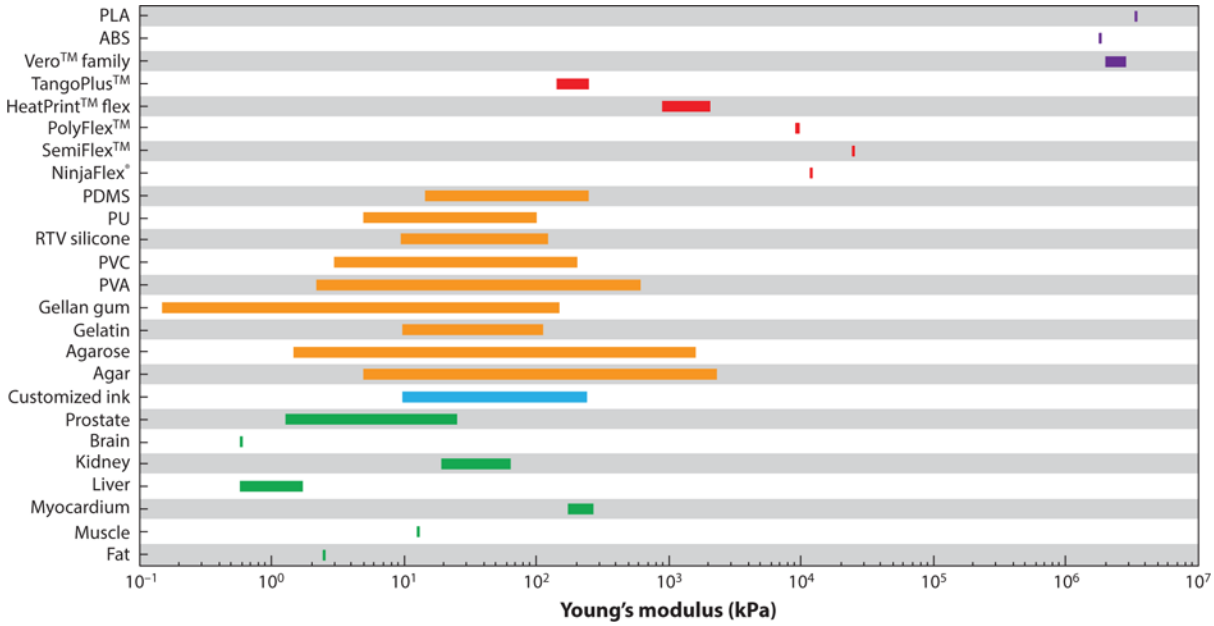


**Figure 6.**

Comparison of Young's modulus of biological tissues (*green*) with different materials including customized polymeric ink (*blue*), tissue-mimicking materials (*orange*), commercial 3D printing elastomeric (rubber-like) materials (*red*), and commercial 3D printing rigid plastics (*purple*). Data for all human biological tissues are retrieved from Reference 46. Myocardium and kidney are porcine tissue retrieved from References 89 and 90, respectively. Data for customized polymeric ink are retrieved from Reference 14. Data for all tissue-mimicking materials are retrieved from Reference 46. Data for commercial 3D printing materials including NinjaFlex®, SemiFlex™, PolyFlex™, HeartPrint™ Flex, TangoPlus™, Vero™ family, and ABS/PLA are retrieved from References 91–97, respectively. Abbreviations: ABS, acrylonitrile butadiene styrene; PDMS, polydimethylsiloxane; PLA, polylactic acid; PU, polyurethane; PVA, polyvinyl alcohol; PVC, polyvinyl chloride; RTV silicone, room-temperature vulcanizing silicone.

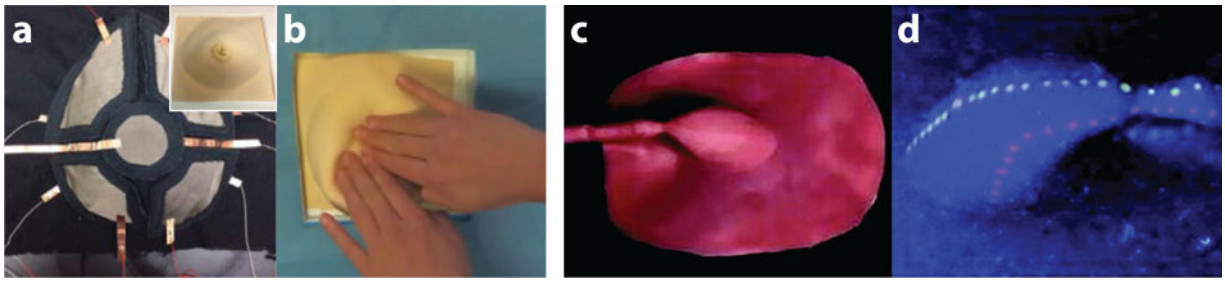


**Figure 7.**

Organ models or simulators with integrated functions. (*a*) Force sensors were shaped to fit a breast model for a breast examination simulator. (*Inset*) Breast examination simulator with an integrated sensor. (*b*) Demonstration of the clinical breast examination on the simulator with integrated force sensor. Panels *a* and *b* adapted with permission from Reference 107. Copyright 2016, IOS Press. (*c,d*) Top view of a pyeloplasty simulator model with the integrated ultraviolet (UV) light–sensitive assessment lines, under room light (*c*) and UV (*d*). Panels *c* and *d* adapted with permission from Reference 108. Copyright 2014, Mary Ann Liebert, Inc.

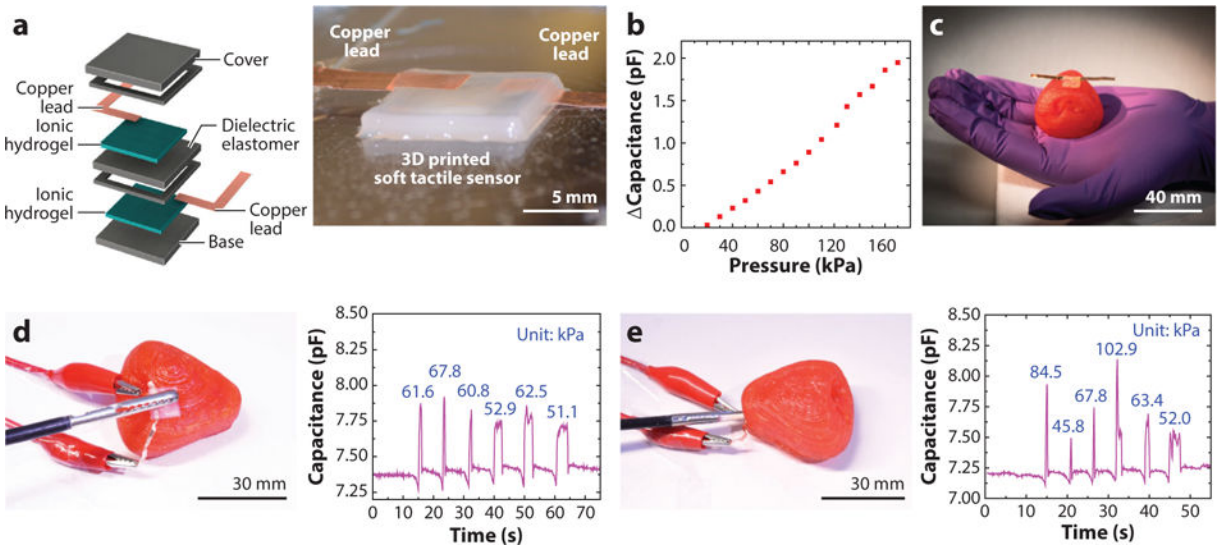


**Figure 8.**

Quantitative surgical rehearsal using the 3D printed prostate model with integrated functionalities. (*a*) Schematic of the structure of the 3D printed soft tactile sensor (*left*) and photograph of the corresponding 3D printed sensor (*right*). (*b*) Calibration of the 3D printed sensor based on the correlation between capacitance change and the applied pressure. (*c)* Photograph of the 3D printed prostate model integrated with the soft tactile sensor. (*d)* Quantitative surgical rehearsal involving the 3D printed prostate model upon applying a surgical grasper on the sensor integrated on the outer surface of the model and its corresponding pressure responses (indicated at each of the peaks) from the capacitance changes of the sensor. (*e*) Quantitative surgical rehearsal involving the 3D printed prostate model when applying surgical scissors on the sensor integrated on the urethra surface inside of the model and its corresponding pressure responses (indicated at each of the peaks) from the capacitance changes of the sensor. Figure adapted with permission from Reference 14. Copyright 2017, John Wiley & Sons.